Contents lists available at ScienceDirect

Saudi Pharmaceutical Journal

Original article

Cepharanthine induces ROS stress in glioma and neuronal cells via modulation of VDAC permeability

Karolina Cierluk [a], Wojciech Szlasa [b], Joanna Rossowska [c], Mounir Tarek [d], Anna Szewczyk [e,f], Jolanta Saczko [e], Julita Kulbacka [e,*]

[a] Faculty of Chemistry, Wroclaw University of Science and Technology, Wroclaw, Poland
[b] Faculty of Medicine, Wroclaw Medical University, Wroclaw, Poland
[c] Hirszfeld Institute of Immunology and Experimental Therapy, Polish Academy of Sciences, Wroclaw, Poland
[d] Université de Lorraine, CNRS, LPCT, F-54000 Nancy, France
[e] Department of Molecular and Cellular Biology, Faculty of Pharmacy, Wroclaw Medical University, Wroclaw, Poland
[f] Department of Animal Developmental Biology, Institute of Experimental Biology, University of Wroclaw, Wroclaw, Poland

ABSTRACT

Cepharanthine (CEP) is a bisbenzylisoquinoline alkaloid. Molecular dynamics studies show that CEP interacts with Voltage-dependent anion channel (VDAC), inducing the voltage-independent channel narrowing. In the new conformation, transport between mitochondria and cytoplasm is altered, which leads to the dose-dependent cytotoxicity.

The biological effects of the interaction were investigated on glioblastoma multiforme (SNB-19) and neuronal (PC-12 + NGF) cell lines. The cytotoxic potential of cepharanthine was determined by MTT assay and flow cytometry apoptosis/necrosis studies. T-type calcium channel and VDAC were labelled by the immunocytochemical method. Additionally, fluorescent labelling of reactive oxygen species and mitochondria was performed. Changes in the pore size of VDAC were calculated as well. Molecular dynamics simulations were carried out to examine the interactions of cepharanthine with VDAC.

The obtained results prove that cepharanthine enhances the apoptosis in glioma and neuronal cells by the release of reactive oxygen species. Cepharanthine alters the mitochondria-to-cytoplasm transport and thus induces the cytotoxicity with no selectivity.

© 2020 The Author(s). Published by Elsevier B.V. on behalf of King Saud University. This is an open access article under the CC BY-NC-ND license (http://creativecommons.org/licenses/by-nc-nd/4.0/).

1. Introduction

Glioma is an intracranial tumour, that severely affects the neural tissue of the brain. The most severe stage of glioma is the glioblastoma multiforme (astrocytoma diffusa), with an average of 15 months of survival of the patients (Hanif et al., 2017). Noticeably, the forms of astrocytomas differ in cancer-associated enzymes activity: the low stages are mostly associated with the overexpression of IDH1 and IDH2 and the further stages with the

loss-of-function mutations in p53 and Rb coding genes and gain-of-function mutations in PI3K kinase genes (Masui et al., 2016).

The treatment methods and prognosis depend on the location of the tumour, the genetic profile, the proliferative activity and the age of the patient (Zhang et al., 2019). The transition from anaplastic astrocytoma to glioblastoma multiforme (GBM), lasts about 3 months in an adult patient (Urbanska et al., 2014). The median of life after diagnosis remains about 14–15 months, which assigns glioblastoma as one of the most acute cancer types (Hanif et al., 2017). GBM is the cause of 2.5% of deaths caused by cancer, the same time being the third leading cause of cancer-related death among people between 15 and 34 years of life (Hanif et al., 2017). Glioblastoma multiforme develops mostly in the brain hemispheres and less likely in the brainstem and cerebellum (Urbanska et al., 2014). Macroscopically, GBM is heterogeneous. The histopathological samples include multifocal haemorrhages, necrosis of the surrounding tissue with cystic and gelatinous areas (Hanif et al., 2017). The characteristic proliferation of endothelial cells in the glomerular structure is a glioblastoma-specific

Production and hosting by Elsevier

morphological property (Hanif et al., 2017). GBM contains numerous molecular modifications compared to a non-cancerous glial cell, for instance, an increased expression of anti-apoptotic and pro-apoptotic proteins (Bax, Bcl-2) (Urbanska et al., 2014). In turn, mutations of the anti-apoptotic Bcl-2, Bcl-xL and Mcl-1 proteins in GBM are responsible for resistance to radiotherapy and chemotherapy (Guntuku et al., 2016).

Voltage-dependent anion channel (VDAC) plays a significant role in GBM development and progression [7]. The channel is located in the outer mitochondrial membrane and acts as a key regulator of communication between mitochondria and the cytoplasm (Colombini, 2012). Moreover, VDAC is a docking station for several cytoplasmic proteins, some of which are involved in the inflammation process (IkB) and glucose metabolism (hexokinase) (Pastorino and Hoek, 2008). Conversely, T-type calcium channel is overexpressed by various cancers (Antal and Martin-Caraballo, 2019; Sallan et al., 2018). It is responsible for the regulation of the Ca^{2+} entry during small repolarizations around the resting potential of the cell membrane (Weiss and Zamponi, 2013). When stimulated by ROS, the channel induces Ca^{2+} shift from the extracellular space to the cytoplasm (Görlach et al., 2015).

Conventional GBM treatment includes chemotherapy, radiotherapy and surgery (Minniti et al., 2009; Perry and Wesseling, 2016). Although the therapies are effective, the rapid tumour progression and secondary resistance to the therapies raise the need for novel therapeutic options (Minniti et al., 2009). Nowadays research focuses on natural drugs with anti-glioma properties (Vengoji et al., 2018). One of the most promising compounds is cepharanthine (CEP) - a bisbenzylisoquinoline alkaloid isolated from the tuber *Stephania cepharantha Hayata* (Huang et al., 2014). It is widely used in the traditional treatment of various diseases e.g. asthma, tuberculosis, cancer, etc (Semwal et al., 2010). Reducing the fluidity of the membrane and therefore the drug resistance mechanisms, CEP intensifies the potency of anti-cancer agents, like Daunomycin, Vincristine and Adriamycin (Schiff, 1991; Shiraishi et al., 1987). Moreover, CEP raises the generation of intracellular reactive oxygen species (ROS), already extensively produced by cancer cells (Aggarwal et al., 2019; Bailly, 2019; Liou and Storz, 2010; Rattanawong et al., 2018). The anti-inflammatory, immunomodulatory, antiallergic, antioxidative and anti-cancer properties support that CEP could be a potential candidate for a novel anti-GBM agent (Kono et al., 2002; Marta Baksalrska-Pazera, 2001; Schiff, 1991; Shiraishi et al., 1987; Urbanska et al., 2014). Aside from the clinical perspectives, the mechanism of CEP cellular action should be studied to provide a proper background for future in vivo research.

This study aimed to evaluate the interactions between VDAC and CEP with its molecular implications. The molecular dynamic study was implemented to simulate the modulation of VDAC channel by CEP under both channel-opening and -closing transmembrane voltages. The biological effects of CEP were evaluated on the SNB-19 (GBM) and PC-12 + NGF (neuronal model) cell lines. CEP was studied in terms of proapoptotic activity and the ability to shift the reactive oxygen species (ROS) to the cytoplasm. The calcium metabolism, accelerated by CEP was assessed by immunocytochemical staining studies of T-type calcium channel and VDAC.

2. Materials and methods

2.1. System preparation and MD simulations

Simulations were performed in GROMACS 2018.3 (Abraham et al., 2015). Systems composed of VDAC (PDB: 2JK4) in a membrane (POPC 70%, CHL1 30%) were built in CHARMM-GUI (Jo et al., 2008). CEP structure was simulated with parameters obtained from CGEN-FF (Vanommeslaeghe et al., 2010). The first system was composed of the channel and the second one of the channel with CEP. The systems were simulated under both channel opening and closing voltages. Before the simulation, the systems were minimized. Afterwards, the systems were equilibrated using the CHARMM-GUI output files. Additionally, the systems were equilibrated under NPT conditions for 100 ns to relax the protein and the membrane and to maintain the surface tension on the membrane-water interface equal to 0, on both sides of the membrane. In the end, the 40 ns MD simulations have been carried under NPT ensemble (303.15 K, 1 atm). The equations of motion were integrated using the multiple time-step algorithms. A time step of 2.0 fs was employed. Chemical bonds between hydrogen and non-hydrogen atoms were constrained to their equilibrium value. Long-range, electrostatic forces were applied by using a fast implementation of the particle mesh Ewald (PME) approach. The systems were simulated under two externally added voltages: 10 and 50 mV. Results were visually analyzed with VMD (Humphrey et al., 1996). The pore size of VDAC was estimated, by analyzing the last 100 frames of the simulation, taking each 10th frame and proceeding it with HOLE software (Smart et al., 1996). All the data was gathered in tables and plotted. The statistical analysis involved the calculations of standard deviations.

2.2. Cell culture

The in vivo experiments were carried on human SNB-19 glioblastoma multiforme and PC-12 cell lines. PC-12 cell line was derived from pheochromocytoma of the rat adrenal medulla from the ECACC, and SNB-19 cell line was purchased from ATCC. Glioblastoma cells were cultured under sterile conditions in Dulbecco's Modified Eagle Medium (DMEM, Sigma-Aldrich, St. Louis, MO), and pheochromocytoma cells were cultured in RPMI 1640 (Sigma-Aldrich, St. Louis, MO). Both media were supplemented with 10% fetal bovine serum (FBS, Sigma-Aldrich) and 20 UI/20 μg/ml penicillin/streptomycin (Sigma-Aldrich). Additionally, to obtain the neuronal model, PC-12 were stimulated with NGF (nerve growth factor). To provide the monolayer growth type, cultures were grown in plastic 25 cm^2 flasks (Falcon, Becton, Dickinson and Co., Franklin Lakes, NJ) and incubated under constant temperature conditions (37 °C), humidity (90%) and CO_2 concentration (5%). The experiments were carried after PC-12 obtained the morphology of the neuronal cells. For the experiments, the cells were removed from the bottles by trypsinization (trypsin 0.25% and EDTA 0.02%, Sigma-Aldrich) and washed with PBS buffer (Bio-Shop, Canada).

2.3. Cells viability assay

Cepharanthine (CEP) cytotoxicity was determined using the MTT assay. For the viability evaluation 0.5, 1, 5, 10 and 20 μM CEP concentrations were used. All dilutions were performed in cultivation media. Cells were trypsinized and seeded in density 2×10^4 on 96-well plates. Cells were cultivated overnight to adhere and afterwards incubated with CEP for 24 h. For longer incubation (72 h) cells were seeded in the density of 5×10^3. For the viability measurements, the medium was replaced with 100 μl, 5 mg/ml (3-(4,5-dimethylthiazol-2-yl)-2,5-diphenyltetrazolium bromide (MTT, Sigma-Aldrich) diluted in phosphate-buffered saline (PBS, Bioshop, Poland) per well for 4 h incubation. 100 μl of 36% acidic isopropyl alcohol (Chempur, Poland) per well has been added and formazan crystals dissolved by vigorous pipetting. The absorbance was measured in the multiplate reader (EnSpire, Perkin Elmer) at a wavelength of 570 nm. The results were presented as a percentage of control untreated cells. Each assay has performed a minimum in eight replicates.

2.4. Flow cytometric cell death analysis

Cell death identification was performed by Annexin V and pro-pidium iodide (PI) assay (BioLegend, Canada) by flow cytometry studies. For the experiments, cells were cultured on 6-well plates for 72 h and 24 h incubation with CEP respectively. The medium was then replaced with fresh medium containing increasing con-centrations of drug (0.5, 5, 10 μM CEP and 200 μM cisplatin - pos-itive control) and was incubated for 24 h and 72 h respectively. Following trypsinization, the cells were treated with 100 μl/well APC-labeled Annexin V/PI diluted in PBS and incubated in the dark for 15 min. Then 200 μl PBS per well has been added and examined using a flow cytometer (BD LSR Fortessa X-20, Becton Dickinson, USA) to obtain the 2-D staining pattern of APC and PI.

2.5. Immunocytochemistry of ion channels

Immunocytochemical staining after 24 h and 72 h incubation with 0.5; 5; 10 μM cepharanthine solutions was performed by the use of Avidin-Biotin Complex (ABC) method. The cells were seeded on 12-well diagnostic microscopic slides (Thermo Fisher Scientific). After incubation, cells were fixed in 4% paraformaldehyde-PBS (PFA, Sigma- Aldrich, USA) solution for 10 min and then stained with the EXPOSE Rabbit Specific HRP/ DAB Detection IHC kit (Abcam, United States; Cat. no. ab80a36). After blocking nonspecific binding sites, cells were incubated over-night at 4 °C with polyclonal anti-rabbit calcium T-channel anti-body (Santa Cruz Biotechnology, Cat. no. sc-25691) diluted 1:200 in PBS buffer and polyclonal anti-rabbit VDAC antibody (ABCAM, no ab34726) diluted 1:400 in PBS buffer. Between particular steps, samples were rinsed with 1% Triton X-100 in PBS. To reveal the cell nuclei, the samples were stained with hematoxylin duting 3 min. The immunocytochemical reaction was analyzed by the upright microscope (Olympus BX43, Japan). The intensity of immunocyto-chemical staining was evaluated according to the following scor-ing: (−) negative, (+) weak, (++) moderate and (+++) strong.

2.6. Fluorescent ROS staining

For immunofluorescent observations, cells were seeded on microscopic cover slides for 24 h incubation with DMEM to adhere. Afterwards, the medium was replaced with a fresh one, containing (or not – control cells) increasing concentrations of drug (0.5, 2.5, 5 μM CEP) and were incubated for 72 h and 24 h respectively. The medium with CEP was removed and alive cells have been stained with 200 nM MitoTracker Green FM (Thermo Fisher Scien-tific) and 200 nM MitoTracker Red CM-H_2XRos (Thermo Fisher Sci-entific) solutions, diluted in DMEM without FBS. The samples were incubated for 30 min. To reveal the cell nuclei, the samples were fixed with Fluoroshield with DAPI (Sigma-Aldrich). MitoTracker Green FM (Thermo Fisher Scientific) dye stains mitochondria; MitoTracker Red CM-H2XRos (Thermo Fisher Scientific) dye fluo-resces upon oxidation, and DAPI dye interact with DNA by intercalation.

2.7. Statistical analysis

Statistical significance was determined by unpaired t-Student tests for cytotoxicity tests and two-way analysis of variance (ANOVA) for the toxicity measurements preceded by cepharan-thine preincubation. Differences between treated samples and con-trol cells not treated with cepharanthine, with $p \leq 0.0001$ considered as a statistically significant. The results were analyzed statistically with the GraphPad Prism 7.0 software. Samples were analyzed in at least four replications in three independent experiments.

3. Results

3.1. VDAC molecular dynamics studies

The molecular dynamics simulations indicate that CEP stimu-lates the narrowing of the pore of VDAC independently on the transmembrane potential. Namely, under channel-opening trans-membrane voltage, the pore of VDAC remains wide. In the same instance, VDAC simulated with CEP, induced the narrowing of the pore (Fig. 1).

The docking studies of CEP to VDAC revealed the differences between CEP localization under various transmembrane voltages. When simulated under channel-closing voltage conditions, the drug localizes on the inner side of the outer mitochondrial mem-brane (OMM). Conversely, when simulated under the channel-opening transmembrane voltage, CEP localizes on the cytoplasmic side of the OMM (Fig. 2).

3.2. Cell viability assay

The mitochondrial activity assay (MTT) was used to evaluate the cytotoxic effect of CEP. The incubation with CEP after 72 h was significantly more cytotoxic than after 24 h exposure. In gen-eral, the PC-12 + NGF cell line was more affected than SNB-19. In 24 h incubation, there was observed a linear decrease in PC-12 cells viability. Conversely, SNB-19 cells were much more resistant and the first significant decrease in viability was observed after application of 20 μM CEP. Interentingly, after 72 h of incubation, both cell lines were highly affected by the application of 5 μM CEP (Fig. 3).

For both cell lines, the IC50 values were calculated and pre-sented in Table 1. Time dependence of the IC50 value was observed for SNB-19 cells, but almost not for PC-12 + NGF cells. Namely, after both incubation times, the neuronal model was characterized by IC50 around 3.3 μM.

3.3. Cell death type analysis

The cell death type was assessed by flow cytometry Annexin-V/ PI assay. After 24 h exposition to CEP, no apoptosis was induced in SNB-19 cells. However, after 72 h of incubation, there was observed an increased level of early apoptosis. Conversely, PC-12 + NGF cells underwent early apoptosis even after 24 h of incu-bation with CEP. With the increase in time of incubation, the effect was highly elevated (Fig. 4).

### 3.4. Immunoanalysis of VDAC1 and T-type calcium channels

The immunocytochemical staining of T-type calcium channel revealed an increased number of immunostained SNB-19 cells with the increasing CEP concentration. The most intense staining reac-tion was observed after exposition to 10 μM CEP. Slightly higher staining intensity was observed with the increasing time of CEP incubation in SNB-19 cell line (Table 2). The expression of the channel was not affected by CEP among PC-12 + NGF cell line (Fig. 5).

In the case of VDAC, there was observed a steady increase in channel expression with the increasing CEP concentration. No time differences in the staining intensity were observed in SNB-19 cell line (Fig. 6). PC-12 + NGF cells increased the VDAC expression in the higher drug concentration in comparison to SNB-19 cells. How-ever, the initial expression was highly elevated in PC-12 cells in comparison to SNB-19 cells (Table 3).
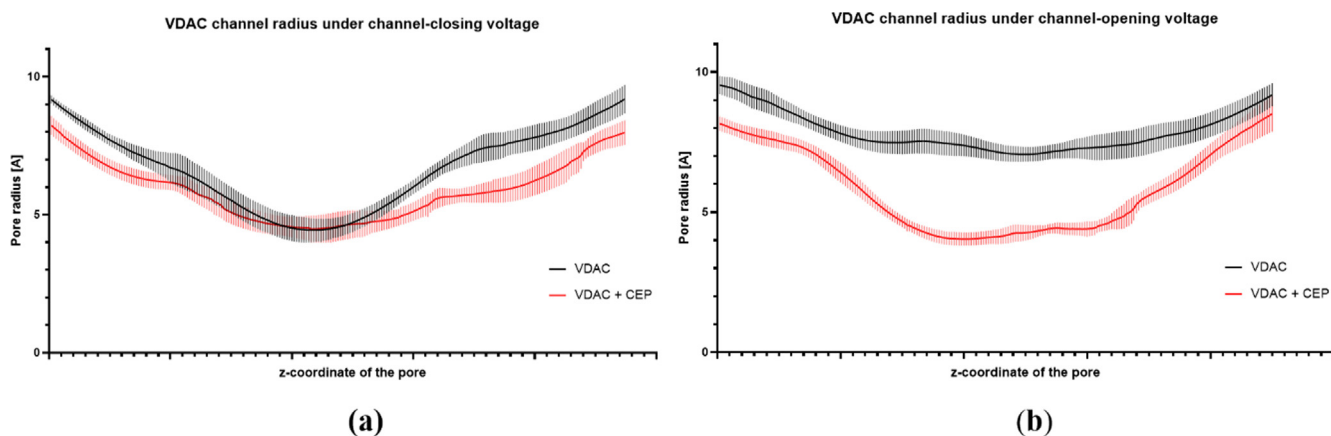
Fig. 1. Pore radius size under (**a**) channel-closing and (**b**) channel-opening voltage analysis (with SDs). The x-axis is the long-axis of the transmembrane channel.
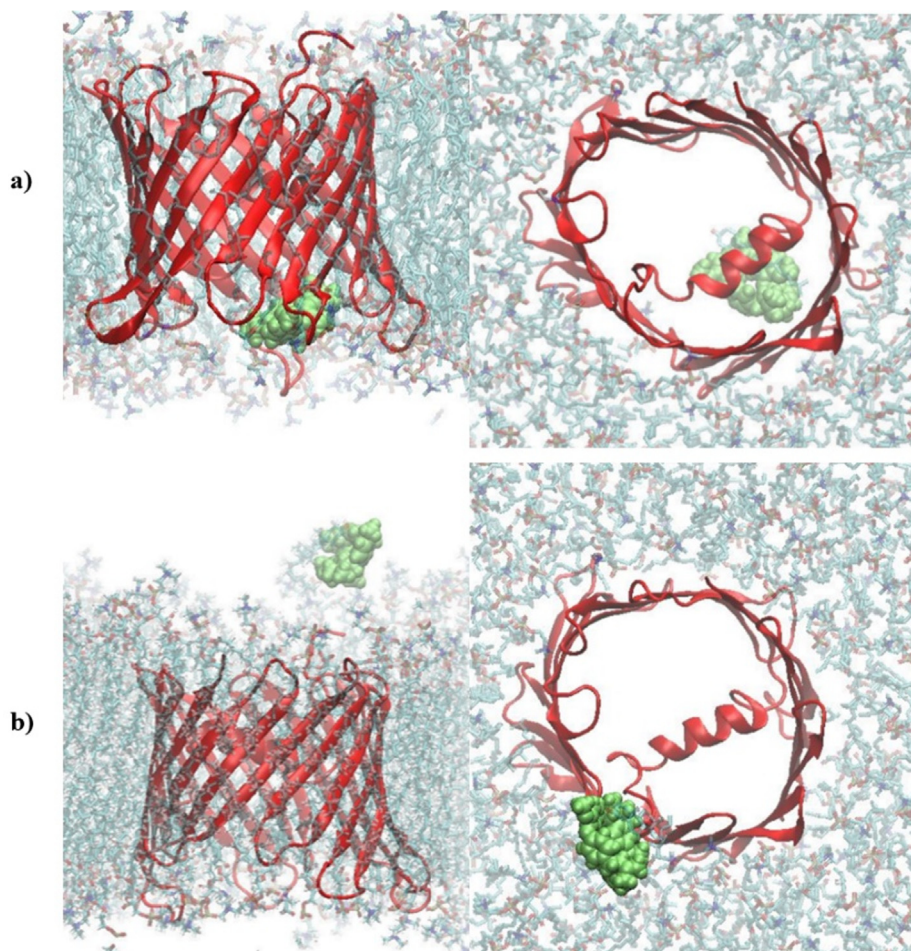
Fig. 2. VDAC-CEP interactions under channel (**a**) closing and (**b**) opening transmembrane voltage conditions (green – CEP, red – VDAC). The channel is situated in the model of the membrane. Both side and top views presented.

3.5. Immunofluorescence detection of reactive oxygen species (ROS)

The comparison of the amount of intracellular ROS in cells incubated with varying CEP concentrations, demonstrated that reactive oxygen species burst with the increasing drug concentration in SNB-19 cell line (Fig. 7). There was observed that with the increasing incubation time, the change in ROS generation cells exposed to lower CEP concentratios. With the addition of CEP, the mitochondrial content becomes more evenly distributed in the cytoplasm in comparison to the more concentrated pattern in control samples.

After 24 h incubation, ROS release in PC-12 + NGF cells was observed in case of a lower concentration of the drug. The tendency of mitochondrial content distribution was comparable to the one in SNB-19 cell line (Fig. 8).
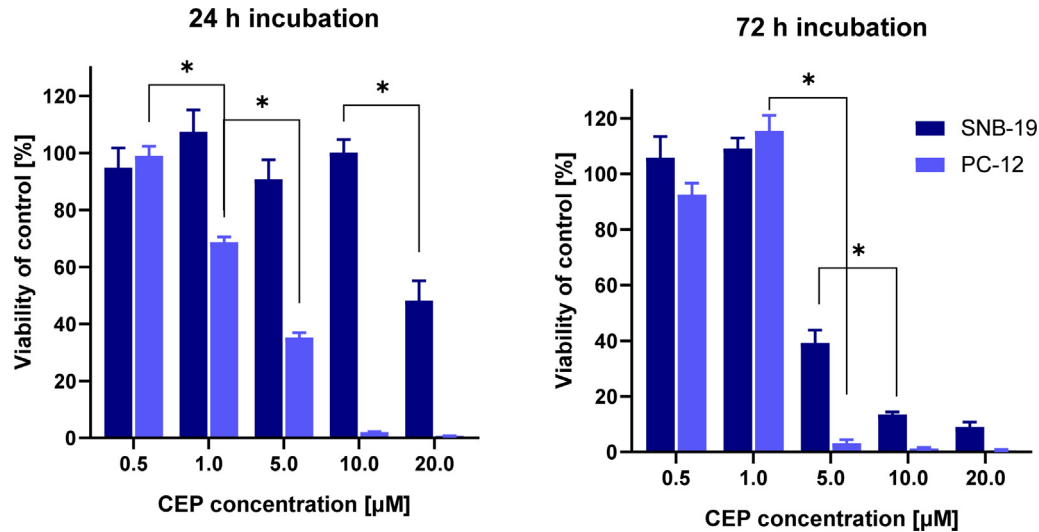
Fig. 3. The viability assay (MTT) after 24 and 72 h incubation with CEP in SNB-19 and PC-12 cells. * $p \leq 0.0001$.

Table 1
CEP - IC50 for SNB-19 and PC-12 cell lines.

Incubation time [h]	IC50 [µM]	
	SNB-19	PC-12
24	19.65	3.24
72	4.38	3.33

4. Discussion

Molecular response to CEP could be explained with molecular dynamics studies. Presented here MD results support the insufficiency of VDAC after incubation with CEP. Namely, its pore is narrowing in response to CEP stimulation. Additionally, the channel remains narrow with no dependence on the transmembrane voltage of OMM. The interactions with CEP occur in different places on different sides of the membrane when simulated under different transmembrane voltages. Experimental studies of the CEP lipophilicity support the postulated displacement to the other side of the membrane (Ma et al., 1991). The dysregulation of VDAC was proved to contribute to the lack of ATP conductance between the

cytoplasm and mitochondria (Colombini, 2012). However, the permeability characteristics of VDAC is confusing. The anionic conductance is favoured when the channel remains in the "opened" state. Conversely, Ca^{2+} and Cytochrome c (Cyt c) conductance is favoured in the "closed" state of the channel (Fang and Maldonado, 2018; Rizzuto et al., 2009). Potentially, the cells incubated with CEP lack in the transport of ATP, glucose and anions between mitochondria and cytoplasm. At the same time, cytotoxic calcium ions are transported throughout the OMM, leading to the mitochondria overload and cell death. Moreover, high overexpression of T-type calcium channel in SNB-19 and low in PC-12 + NGF increases the calcium content in the cytoplasm allowing for the activation of apoptosis and intensification of mitochondrial-calcium overload (Huc et al., 2009; Weiss and Zamponi, 2013).

The narrow conformation of the channel induces the ROS outflow from the intramembranous compartment of the mitochondria. One of the most prominent radical species in the mitochondria that could potentially be transported by VDAC is the proapoptotic Cyt c. The hemoprotein accounts for the increase in the cytoplasmic ROS content (Tan, 2012). The elevated permeability to Cyt c does not only induce ROS-stress but also results in the formation of the apoptosome, composed of Cyt c, Apaf-1
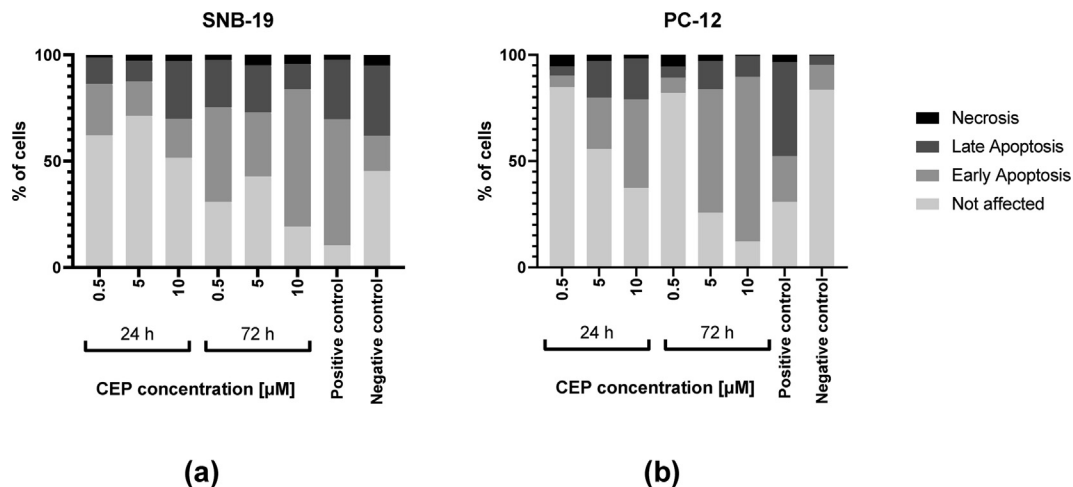

Fig. 4. Cell death analysis in (a) SNB-19 and (b) PC-12 cells after 24 h and 72 h incubation with CEP. the y-axis represents the % of cells in each death type; positive control induced by cisplatin, negative control – stained but CEP untreated cells.

Table 2
The results from immunocytochemical T-type calcium channel staining analysis.

| CEP concentration [μM] | PC-12 + NGF | | SNB-19 | | | |
| | 24 h | | 24 h | | 72 h | |
	Reaction intensity	% of stained cells	Reaction intensity	% of stained cells	Reaction intensity	% of stained cells
0	++	50	−/+	80	−/+	92
0.5	++	50	+	89	+/++	97
5	++	50	+	95	++	100
10	++	50	+++	100	++	100
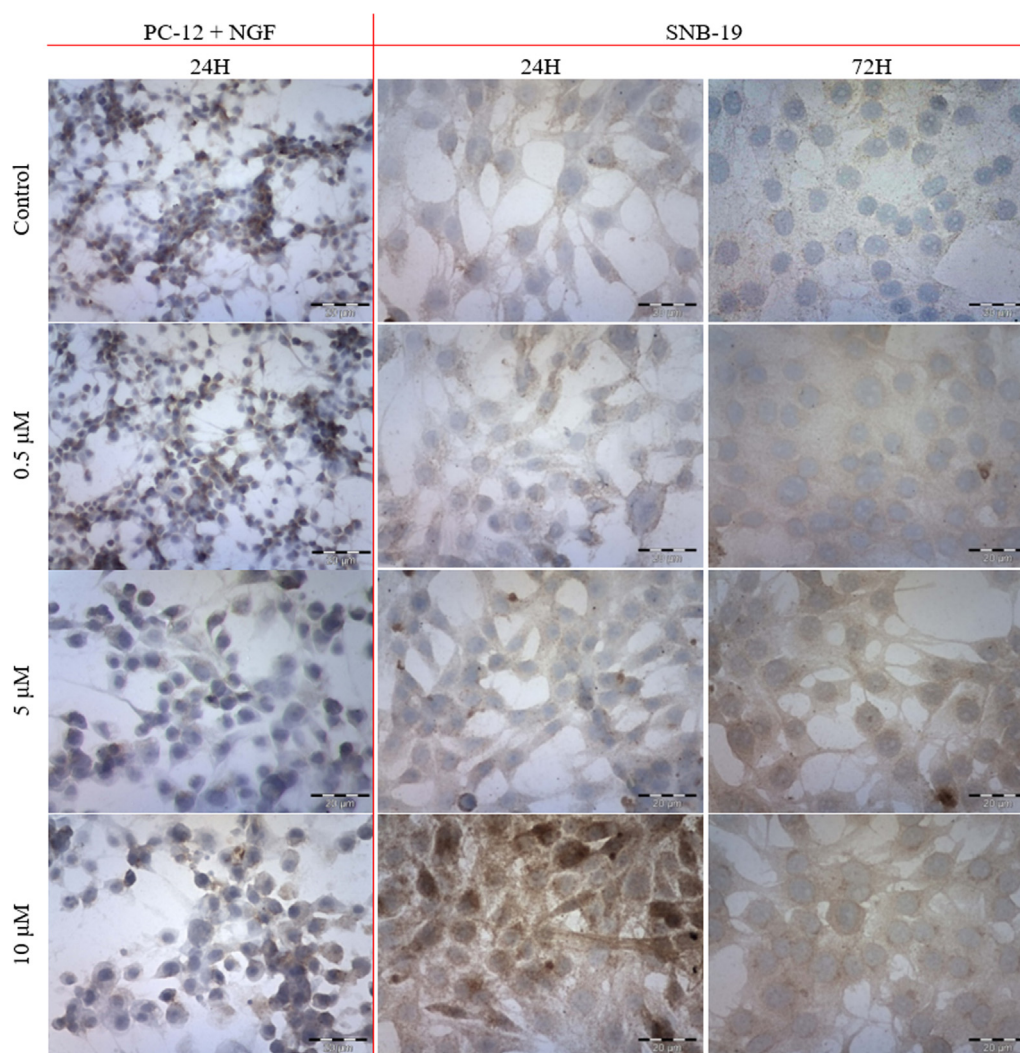
Fig. 5. The immunocytochemical evaluation of calcium T-type channel with ABC technique after 24 h and 72 h incubation (first and second column respectively) with varying concentrations of CEP.

and procaspase-9 (Yuan et al., 2010). This could explain why the incubation with CEP results in the increased apoptosis, without any significant effects on necrosis, which can be seen from cell death type analysis.

The viability results prove that CEP applied in micromolar concentrations is a highly potent cytotoxic agent. Both SNB-19 and PC-12 + NGF were highly apoptotic after the incubation with CEP. Neuronal cells mostly underwent early apoptosis with almost the lack of other cell death type. In contrast, the SNB-19 cells were characterized by the high level of late apoptosis – especially after treatment with higher CEP concentrations. Other researchers also investigated the potency of CEP as an anti-cancer agent on various

cell lines, for instance on cholangiocytoma (KKU-M213), chemosensitive CaOV-3 and chemoresistant OVCAR-3 ovarian cancer cell lines (Harada et al., 2009; Payon et al., 2019; Seubwai et al., 2010). Interestingly, the cytotoxic effect could potentially be translated to the living organism, though the research carried on nude mice also revealed the high efficiency of CEP as an inhibitor of cancer growth (Harada et al., 2009). However, from a clinical point, the chemotherapeutic agent should affect only the neoplasm, omitting the normal cells. Unfortunately, CEP affected the model of the normal neuronal cells more than the GMB, limiting the application of the compound in the systemic treatment. In both mitochondrial activity and cell death studies, the compound was more toxic
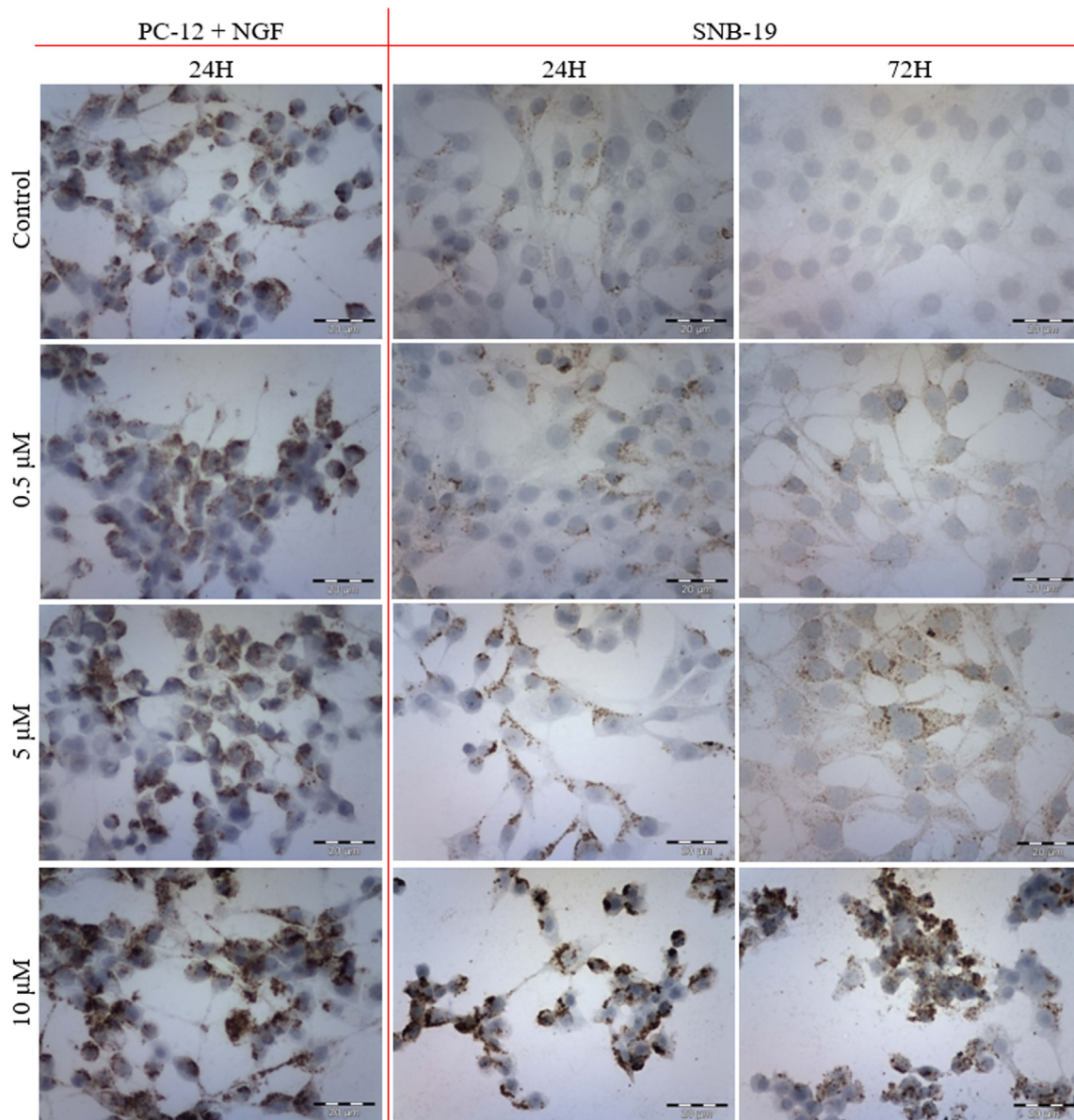
Fig. 6. The immunocytochemical evaluation of VDAC with ABC technique after 24 h and 72 h incubation (first and second column respectively) with varying concentrations of CEP.

Table 3
The results from immunocytochemical VDAC staining analysis.

| CEP concentration [μM] | PC-12 + NGF | | SNB-19 | | | |
| | 24 h | | 24 h | | 72 h | |
	Reaction intensity	% of stained cells	Reaction intensity	% of stained cells	Reaction intensity	% of stained cells
0	++	50	–	No reaction	–	No reaction
0.5	++	50	+	25	+	25
5	++	50	++	50	++	50
10	+++	75	+++	75	+++	75

towards the neuronal cells. Moreover, other researchers proved the bimodal effect of cepharanthine on glioma cell lines (U87MG, U251MG, T98G). Namely in the concentration range of 1–10 μM, CEP stimulated the growth of cancer cells, while in concentrations above 15 μM, CEP induced apoptosis (Kono et al., 2002). Other studies showed that CEP may act as a selective stimulator of prolif-

eration among one type of the cells (Bailly, 2019; Madaan et al., 2018; Tanigaki-Obana and Ito, 1992; Xu, 2016).

In the fluorescent microscopy experiments, CEP induced ROS accumulation in the cytoplasm of the cells. Moreover, the ROS-burst occurred in lower concentration and after lower incubation time in neuronal cells than in GBM. Besides, there were observed
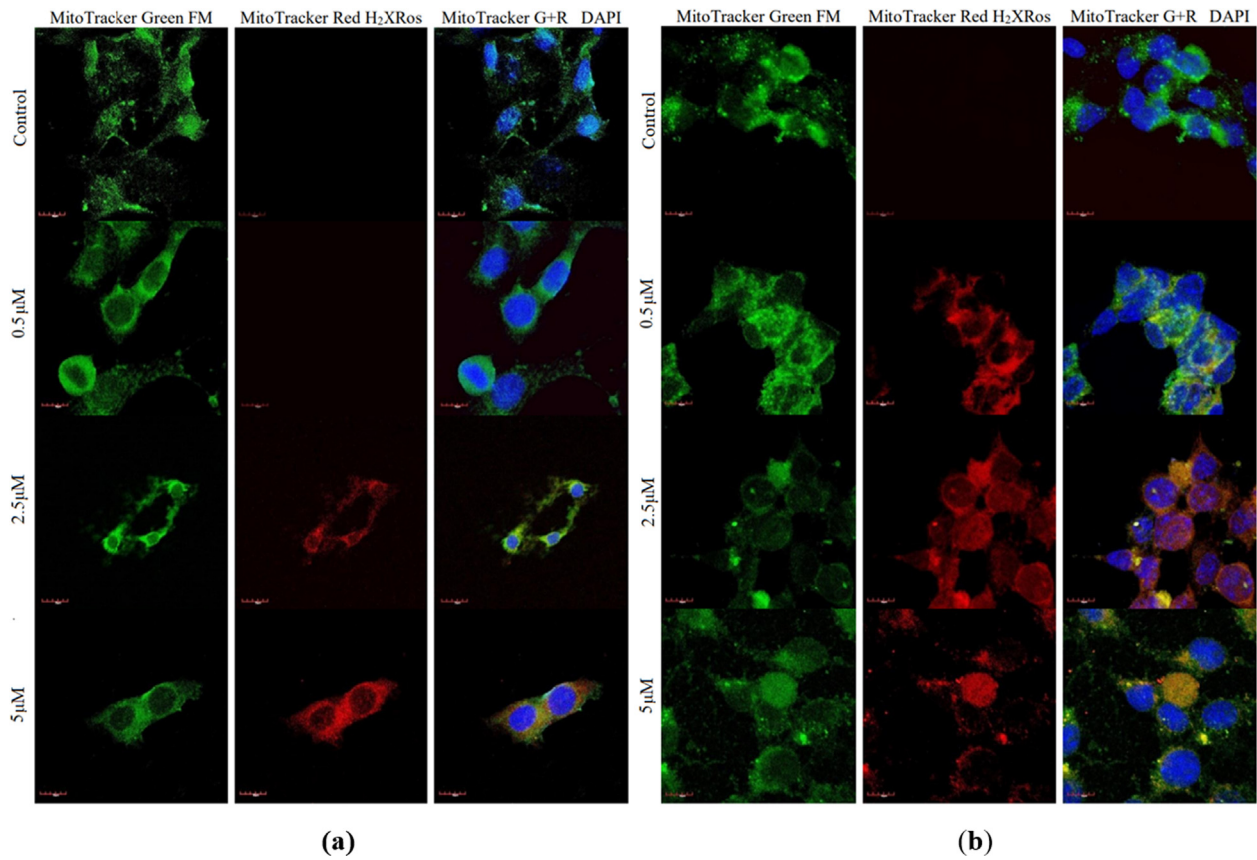
Fig. 7. Immunofluorescent staining of ROS in SNB-19 cells after (**a**) 24 h and (**b**) 72 h of incubation with varying CEP concentrations.
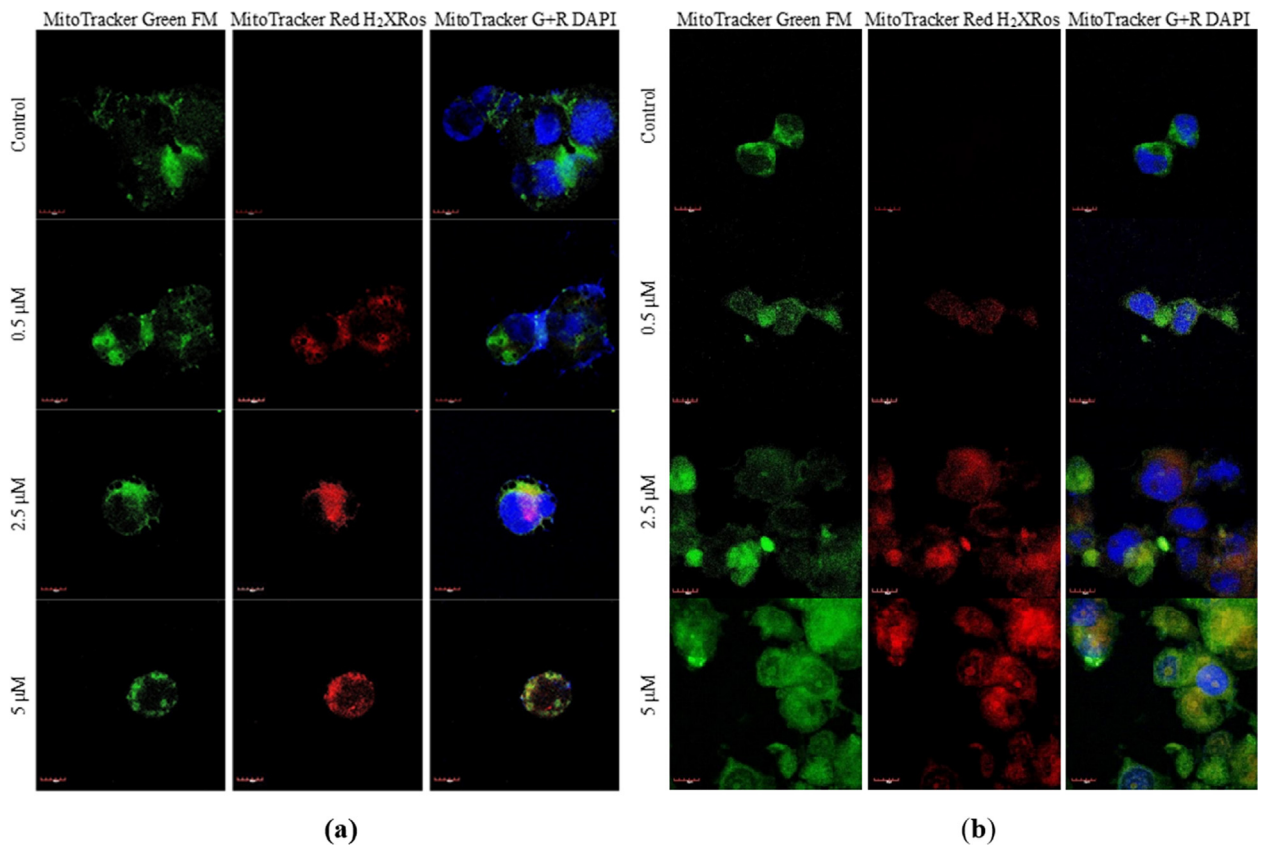

Fig. 8. Immunofluorescent staining of ROS in PC-12 + NGF cells after (**a**) 24 h and (**b**) 72 h of incubation with varying CEP concentrations.

alternations in mitochondrial content and its distribution in the cells. The results support the mitochondria-targeting nature of the compound (Hua et al., 2015). Moreover, the expression of VDAC was also affected by CEP, meaning that the compound interacts with the protein on some level.

In our studies, CEP induced the overexpression of VDAC and T-type calcium channel in SNB-19 cell line. In comparison, among PC-12 + NGF cells both of the channels were not as highly affected – the expression of VDAC was increased only in high (5 μM) concentration. The overexpression of the channels could be a result of their function impairment by CEP. In response, the genetic mechanisms could induce the biosynthesis of the additional proteins to overcome the problem. Interestingly, the cancer cells exhibited a lower initial expression of both channels. With the increased number of targets for cepharanthine in PC-12, the cells remained more sensitive towards incubation with CEP. The results correlated with the higher cytotoxic effect on the normal cells in comparison to cancer.

5. Conclusions

Due to the antiproliferative effects of CEP in relatively low concentrations, the natural compound seems to be a potent cytotoxic agent. By the direct interactions with VDAC, CEP induces the constant pore closure, leading to the ROS outflow to the cytoplasm with the lack of calcium accumulation. High potency in low concentrations and the lack of necrosis inducing properties could potentially lead to the introduction of the drug to the clinical management in the future. Although potent, the compound lacks the selectivity towards GBM.

Future studies concerning interactions of CEP with other targets are necessary to find a proper application for such a potent substance.

Funding

CRediT authorship contribution statement

Karolina Cierluk: Conceptualization, Methodology, Investigation, Data curation, Writing - original draft. **Wojciech Szlasa:** Conceptualization, Methodology, Investigation, Data curation, Writing - original draft. **Joanna Rossowska:** Data curation, Writing - review & editing. **Mounir Tarek:** Methodology, Writing - review & editing, Supervision. **Anna Szewczyk:** Data curation. **Jolanta Saczko:** Writing - review & editing, Funding acquisition. **Julita Kulbacka:** Conceptualization, Methodology, Writing - review & editing, Supervision, Funding acquisition.

Declaration of Competing Interest

The authors declare that they have no known competing financial interests or personal relationships that could have appeared to influence the work reported in this paper.

Acknowledgements

References

Abraham, M.J., Murtola, T., Schulz, R., Páll, S., Smith, J.C., Hess, B., Lindah, E., 2015. Gromacs: High performance molecular simulations through multi-level parallelism from laptops to supercomputers. SoftwareX 1–2, 19–25. https://doi.org/10.1016/j.softx.2015.06.001.

Aggarwal, V., Tuli, H.S., Varol, A., Thakral, F., Yerer, M.B., Sak, K., Varol, M., Jain, A., Khan, M.A., Sethi, G., 2019. Role of reactive oxygen species in cancer progression: Molecular mechanisms and recent advancements. Biomolecules. https://doi.org/10.3390/biom9110735.

Antal, L., Martin-Caraballo, M., 2019. T-type calcium channels in cancer. Cancers (Basel). https://doi.org/10.3390/cancers11020134.

Bailly, C., 2019. Cepharanthine: An update of its mode of action, pharmacological properties and medical applications. Phytomedicine. https://doi.org/10.1016/j.phymed.2019.152956.

Colombini, M., 2012. VDAC structure, selectivity, and dynamics. Biochim. Biophys. Acta - Biomembr. https://doi.org/10.1016/j.bbamem.2011.12.026.

Fang, D., Maldonado, E.N., 2018. VDAC Regulation: A Mitochondrial Target to Stop Cell Proliferation. In: Advances in Cancer Research. Academic Press Inc., pp. 41–69. https://doi.org/10.1016/bs.acr.2018.02.002.

Görlach, A., Bertram, K., Hudecova, S., Krizanova, O., 2015. Calcium and ROS: A mutual interplay. Redox Biol. https://doi.org/10.1016/j.redox.2015.08.010.

Guntuku, L., Naidu, V.G.M., Ganesh Yerra, V., 2016. Mitochondrial Dysfunction in Gliomas: Pharmacotherapeutic Potential of Natural Compounds. Curr. Neuropharmacol. 14, 567–583. https://doi.org/10.2174/1570159x14666160121115641.

Hanif, F., Muzaffar, K., Perveen, K., Malhi, S.M., Simjee, S.U., 2017. Glioblastoma multiforme: A review of its epidemiology and pathogenesis through clinical presentation and treatment. Asian Pacific. J Cancer Prev.

Harada, K., Ferdous, T., Itashiki, Y., Takii, M., Mano, T., Mori, Y., Ueyama, Y., 2009. Effects of cepharanthine alone and in combination with fluoropyrimidine anticancer agent, S-l, on tumor growth of human oral squamous cell carcinoma xenografts in nude mice. Anticancer Res. 29, 1263–1270.

Hua, P., Sun, M., Zhang, G., Zhang, Y., Tian, X., Li, X., Cui, R., Zhang, X., 2015. Cepharanthine induces apoptosis through reactive oxygen species and mitochondrial dysfunction in human non-small-cell lung cancer cells. Biochem. Biophys. Res. Commun. 460, 136–142. https://doi.org/10.1016/j.bbrc.2015.02.131.

Huang, H., Hu, G., Wang, C., Xu, H., Chen, X., Qian, A., 2014. Cepharanthine, an alkaloid from Stephania cepharantha Hayata, inhibits the inflammatory response in the RAW264.7 cell and mouse models. Inflammation 37, 235–246. https://doi.org/10.1007/s10753-013-9734-8.

Huc, S., Monteil, A., Bidaud, I., Barbara, G., Chemin, J., Lory, P., 2009. Regulation of T-type calcium channels: Signalling pathways and functional implications. Biochim. Biophys. Acta - Mol. Cell Res. https://doi.org/10.1016/j.bbamcr.2008.11.003.

Humphrey, W., Dalke, A., Schulten, K., 1996. VMD: Visual molecular dynamics. J. Mol. Graph. 14, 33–38. https://doi.org/10.1016/0263-7855(96)00018-5.

Jo, S., Kim, T., Iyer, V.G., Im, W., 2008. CHARMM-GUI: A web-based graphical user interface for CHARMM. J. Comput. Chem. 29, 1859–1865. https://doi.org/10.1002/jcc.20945.

Kono, K., Takahashi, J.A., Ueba, T., Mori, H., Hashimoto, N., Fukumoto, M., 2002. Effects of combination chemotherapy with biscoclaurine-derived alkaloid (Cepharanthine) and nimustine hydrochloride on malignant glioma cell lines. J. Neurooncol. 56, 101–108. https://doi.org/10.1023/A:1014548618440.

Liou, G.Y., Storz, P., 2010. Reactive oxygen species in cancer. Free Radic. Res. https://doi.org/10.3109/10715761003667554.

Ma, J.K.H., Mo, C.G., Malanga, C.J., Ma, J.Y.C., Castranova, V., 1991. Binding of bisbenzylisoquinoline alkaloids to phosphatidylcholine vesicles and alveolar macrophages: Relationship between binding affinity and antifibrogenic potential of these drugs. Exp. Lung Res. 17, 1061–1077. https://doi.org/10.3109/01902149109064335.

Madaan, A., Verma, R., Singh, A.T., Jaggi, M., 2018. Review of Hair Follicle Dermal Papilla cells as in vitro screening model for hair growth. Int. J. Cosmet. Sci. 40, 429–450. https://doi.org/10.1111/ics.12489.

Marta Baksalrska-Pazera, G.N., 2001. Widok NGF na szlaku, czyli przekazywanie sygnału troficznego w neuronie. Kosm. Probl. Nauk Biol. 50, 250–251.

Masui, K., Mischel, P.S., Reifenberger, G., 2016. Molecular classification of gliomas, in: Handbook of Clinical Neurology. Elsevier B.V., pp. 97–120. https://doi.org/10.1016/B978-0-12-802997-8.00006-2.

Minniti, G., Muni, R., Lanzetta, G., Marchetti, P., Maurizi Enrici, R., 2009. Chemotherapy for glioblastoma: Current treatment and future perspectives for cytotoxic and targeted agents. Anticancer Res.

Pastorino, J.G., Hoek, J.B., 2008. Regulation of hexokinase binding to VDAC. J. Bioenerg. Biomembr. 40, 171–182. https://doi.org/10.1007/s10863-008-9148-8.

Payon, V., Kongsaden, C., Ketchart, W., Mutirangura, A., Wonganan, P., 2019. Mechanism of Cepharanthine Cytotoxicity in Human Ovarian Cancer Cells. Planta Med. 85, 41–47. https://doi.org/10.1055/a-0706-7503.

Perry, A., Wesseling, P., 2016. Histologic classification of gliomas, in: Handbook of Clinical Neurology. Elsevier, pp. 71–95. https://doi.org/10.1016/B978-0-12-802997-8.00005-0.

Rattanawong, A., Payon, V., Limpanasittikul, W., Boonkrai, C., Mutirangura, A., Wonganan, P., 2018. Cepharanthine exhibits a potent anticancer activity in p53-mutated colorectal cancer cells through upregulation of p21Waf1/Cip1. Oncol. Rep. 39, 227–238. https://doi.org/10.3892/or.2017.6084.

Rizzuto, R., Marchi, S., Bonora, M., Aguiari, P., Bononi, A., De Stefani, D., Giorgi, C., Leo, S., Rimessi, A., Siviero, R., Zecchini, E., Pinton, P., 2009. Ca2+ transfer from the ER to mitochondria: When, how and why. Biochim. Biophys. Acta - Bioenerg. https://doi.org/10.1016/j.bbabio.2009.03.015.

Sallan, M.C., Visa, A., Shaikh, S., Nager, M., Herreros, J., Cantí, C., 2018. T-type Ca2+ Channels: T for targetable. Cancer Res. https://doi.org/10.1158/0008-5472.CAN-17-3061.

Schiff, P.L., 1991. Bisbenzylisoquinoline Alkaloids. J. Nat. Prod. 54, 645–749. https://doi.org/10.1021/np50075a001.

Semwal, D.K., Badoni, R., Semwal, R., Kothiyal, S.K., Singh, G.J.P., Rawat, U., 2010. The genus Stephania (Menispermaceae): Chemical and pharmacological perspectives. J. Ethnopharmacol. https://doi.org/10.1016/j.jep.2010.08.047.

Seubwai, W., Vaeteewoottacharn, K., Hiyoshi, M., Suzu, S., Puapairoj, A., Wongkham, C., Okada, S., Wongkham, S., 2010. Cepharanthine exerts antitumor activity on cholangiocarcinoma by inhibiting NF-κB. Cancer Sci. 101, 1590–1595. https://doi.org/10.1111/j.1349-7006.2010.01572.x.

Shiraishi, N., Akiyama, S., Nakagawa, M., Kobayashi, M., Kuwano, M., 1987. Effect of bisbenzylisoquinoline (biscoclaurine) alkaloids on multidrug resistance in KB human cancer cells. Cancer Res. 47, 2413–2416.

Smart, O.S., Neduvelil, J.G., Wang, X., Wallace, B.A., Sansom, M.S.P., 1996. HOLE: A program for the analysis of the pore dimensions of ion channel structural models. J. Mol. Graph. 14, 354–360. https://doi.org/10.1016/S0263-7855(97)00009-X.

Tan, W., 2012. VDAC blockage by phosphorothioate oligonucleotides and its implication in apoptosis. Biochim. Biophys. Acta - Biomembr. https://doi.org/10.1016/j.bbamem.2011.12.032.

Tanigaki-Obana, N., Ito, M., 1992. Effects of cepharanthine and minoxidil on proliferation, differentiation and keratinization of cultured cells from the murine hair apparatus. Arch. Dermatol. Res. 284, 290–296. https://doi.org/10.1007/BF00372583.

Urbanska, K., Sokolowska, J., Szmidt, M., Sysa, P., 2014. Glioblastoma multiforme - An overview. Wspolczesna Onkol. https://doi.org/10.5114/wo.2014.40559.

Vanommeslaeghe, K., Hatcher, E., Acharya, C., Kundu, S., Zhong, S., Shim, J., Darian, E., Guvench, O., Lopes, P., Vorobyov, I., Mackerell, A.D., 2010. CHARMM general force field: A force field for drug-like molecules compatible with the CHARMM all-atom additive biological force fields. J. Comput. Chem. 31, 671–690. https://doi.org/10.1002/jcc.21367.

Vengoji, R., Macha, M.A., Batra, S.K., Shonka, N.A., 2018. Natural products: A hope for glioblastoma patients. Oncotarget. https://doi.org/10.18632/oncotarget.25175.

Weiss, N., Zamponi, G.W., 2013. Control of low-threshold exocytosis by T-type calcium channels. Biochim. Biophys. Acta - Biomembr. https://doi.org/10.1016/j.bbamem.2012.07.031.

Xu, X., 2016. Recent Progresses in Hair Research. Hair Ther Transpl. 6, 110. https://doi.org/10.4172/2167-0951.1000e110.

Yuan, S., Yu, X., Topf, M., Ludtke, S.J., Wang, X., Akey, C.W., 2010. Structure of an apoptosome-procaspase-9 CARD complex. Structure 18, 571–583. https://doi.org/10.1016/j.str.2010.04.001.

Zhang, H., Wang, R., Yu, Y., Liu, J., Luo, T., Fan, F., 2019. Glioblastoma treatment modalities besides surgery. J. Cancer. https://doi.org/10.7150/jca.32475.